New Journal of Physics
The open access journal at the forefront of physics

Deutsche Physikalische Gesellschaft DPG
IOP Institute of Physics

Published in partnership with: Deutsche Physikalische Gesellschaft and the Institute of Physics

OPEN ACCESS

RECEIVED
20 April 2020

ACCEPTED FOR PUBLICATION
21 May 2020

PUBLISHED
17 August 2020

Original content from this work may be used under the terms of the Creative Commons Attribution 4.0 licence.

Any further distribution of this work must maintain attribution to the author(s) and the title of the work, journal citation and DOI.

PAPER

Autoionization dynamics of helium nanodroplets resonantly excited by intense XUV laser pulses

Y Ovcharenko[1,2,12], A C LaForge[3], B Langbehn[1], O Plekan[4], R Cucini[4], P Finetti[4], P O'Keeffe[5], D Iablonskyi[6], T Nishiyama[7], K Ueda[6], P Piseri[8], M Di Fraia[4], R Richter[4], M Coreno[4,5], C Callegari[4], K C Prince[4,9], F Stienkemeier[3,10], T Möller[1,12] and M Mudrich[11,12]

[1] Institut für Optik und Atomare Physik, TU Berlin, 10623 Berlin, Germany
[2] European XFEL GmbH, 22607 Hamburg, Germany
[3] Physikalisches Institut, Universität Freiburg, 79104 Freiburg, Germany
[4] Elettra-Sincrotrone Trieste, 34149 Basovizza, Trieste, Italy
[5] ISM-CNR, Area della Ricerca di Roma 1, Monterotondo Scalo 00015, Italy
[6] Institute of Multidisciplinary Research for Advanced Materials, Tohoku University, 980-8577 Sendai, Japan
[7] Division of Physics and Astronomy, Graduate School of Science, Kyoto University, 606-8501 Kyoto, Japan
[8] CIMAINA and Dipartimento di Fisica, Università degli Studi di Milano, 20133 Milano, Italy
[9] Centre for Translational Atomaterials, and Department of Chemistry and Biotechnology, Swinburne University of Technology, Melbourne, Australia
[10] Freiburg Institute of Advanced Studies (FRIAS), University of Freiburg, 79194 Freiburg, Germany
[11] Department of Physics and Astronomy, Aarhus University, 8000 C Aarhus, Denmark
[12] Authors to whom any correspondence should be addressed.

E-mail: thomas.moeller@physik.tu-berlin.de, yevheniy.ovcharenko@xfel.eu and mudrich@phys.au.dk

Keywords: He nanodroplets, interatomic Coulombic decay, collective autoionization, nanoplasma

Abstract

The ionization dynamics of helium droplets irradiated by intense, femtosecond extreme ultraviolet (XUV) pulses is investigated in detail by photoelectron spectroscopy. Helium droplets are resonantly excited to atomic-like 2p states with a photon energy of 21.5 eV and autoionize by interatomic Coulombic decay (ICD). A complex evolution of the electron spectra as a function of droplet size (250 to 10^6 He atoms per droplet) and XUV intensity (10^9–10^{12} W cm^{-2}) is observed, ranging from narrow atomic-like peaks that are due to binary autoionization, to an unstructured feature characteristic of electron emission from a nanoplasma. The experimental results are analyzed and interpreted with the help of a numerical simulation based on rate equations taking into account all relevant processes—multi-step ionization, electronic relaxation, ICD, secondary inelastic collisions, desorption of electronically excited atoms, and collective autoionization (CAI).

1. Introduction

The rapid development of short-wavelength free-electron lasers (FELs) [1–3] over recent decades has stimulated the investigation of the interaction between intense, high-energy light pulses and matter, and indeed has become a very active field of research in atomic and molecular science [4–6]. In pioneering experimental and theoretical studies, various new phenomena such as absorption enhancement [4, 7] and bleaching [6, 8, 9] as well as modification [10] and suppression [11] of electron emission have been discovered.

A detailed understanding of these mechanisms is of fundamental interest and particularly important for future studies using novel light sources such as x-ray free-electron lasers (FELs). FELs are expected to open new fields in spectroscopy and x-ray imaging, such as recording movies of ultrafast processes and chemical reactions [12]. Depending on the power density, samples can absorb a large number of photons and thus be transformed into highly excited, non-equilibrium systems within femtoseconds, which then undergo complex relaxation. In this context, atomic clusters play an important role as well-controlled model systems.

© 2020 The Author(s). Published by IOP Publishing Ltd on behalf of the Institute of Physics and Deutsche Physikalische Gesellschaft

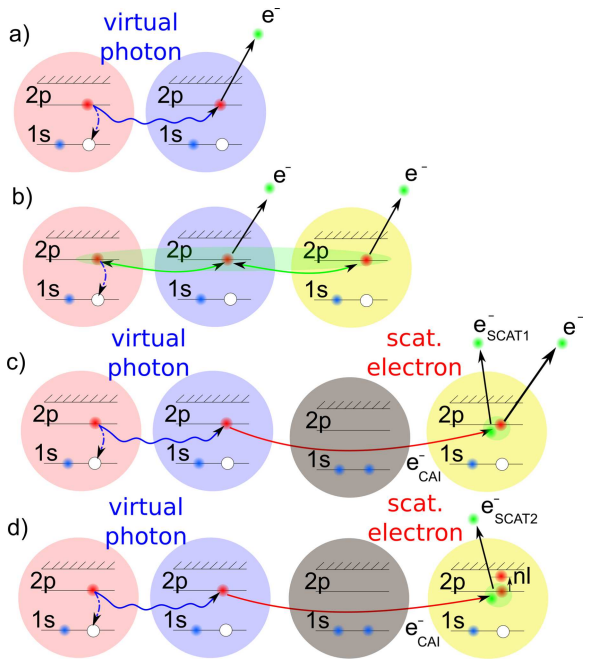

Figure 1. Schematic diagram of (a) ICD of two excited He atoms [14], (b) CAI type process involving three excited He atoms, and (c), (d) CAI with electron scattering on a third excited atom [26].

Tuning their size allows us to investigate *intra-atomic* vs *inter-atomic* relaxation mechanisms and even collective phenomena, thus bridging the gap between molecular and condensed matter physics.

When a nanoscale object (e.g. a large molecule or cluster) absorbs more than one photon, ultrafast energy exchange between the constituent particles is expected to crucially impact the relaxation dynamics. Ionization by intense XUV pulses is heavily influenced by complex electron dynamics, due to either multi-electron collisions with energy exchange [10] or autoionization processes related to interatomic Coulombic decay (ICD) [13], as predicted recently [14]. ICD is a very efficient electronic decay mode of atoms or molecules embedded in an environment. Ionization becomes possible because of energy or charge exchange between the constituents. The discovery of ICD [15–17] has revealed a plethora of related phenomena, involving both energy and electron transfer initiated by single or multiple ionization, as well as by inner- or outer-valence excitation [15]. According to the work by Kuleff *et al* [14], clusters resonantly irradiated by intense light pulses with photon energy insufficient to ionize the atoms by single photon absorption, can efficiently autoionize because of energy or charge exchange between two excited atoms, i.e.:

$$A^* \cdots A^* \rightarrow A \cdots A^+ + e^-. \tag{1}$$

This is experimentally equivalent to Penning ionization [18] for the case that one electronically excited atom ionizes another excited atom. Penning ionization, which was already discovered in the early days of atomic physics [19], usually proceeds in a collision of an excited atom with an atom or molecule with lower ionization potential. While ICD processes have recently moved into the focus of interest of FEL science, we note that similar processes have already been discussed in other scientific contexts, e.g. Penning ionization by atoms in short lived, dipole allowed excited states [20, 21], enhanced ionization by exciton fusion of molecular clusters [22], or in the context of autoionization and fluorescence quenching of nanoparticles [23]. In the various models the ionization rate sensitively depends on the mechanism, namely electron exchange or energy transfer [21, 24], and thus on the distance between the excited species [14]. In the following, we refer for simplicity to ICD since this term is well established in the field of FEL science, although a description in terms of Penning ionization is equivalent [25].

In ICD, neighbouring excited atoms exchange charge or energy resulting in the ionization and emission of an electron from the cluster (figure 1(a)). After excitation of two He atoms into 2p states, one of the 2p electrons decays to the 1s hole and the energy is transferred to the neighbouring 2p excited atom which is then ionized. At large distances between the excited atoms, this preferentially takes place through a virtual photon [14], while at short distances the atomic orbital overlap and charge exchange dominates [25]. In extended systems such as He nanodroplets, this process can already take place at rather low power density, e.g. when using synchrotron radiation [18]. If the power density is sufficiently high ($>10^{10}$ W cm^{-2}, depending on the system), additional processes can occur since a high density of excited atoms is generated

inside the droplet. A selection of the most likely processes involving more than two excited atoms is sketched in figures 1(b)–(d). After autoionization, the free electron either ionizes a third excited atom (figure 1(c)) or promotes the excited electron to higher Rydberg states (figure 1(d)). In the case that three excited atoms are in direct contact (figure 1(b)), inelastic collisions are expected to be even more efficient and dominant [26]. All of these processes lead to a shifting and broadening of the photoemission line measured in the regime of binary ICD. When the ICD electron undergoes many inelastic collisions in a highly excited cluster the direct ionization process, i.e. the characteristic photoline, can be completely quenched [26].

Since all of these processes are based on the sequential absorption of single photons by a transition with a large cross section, they are very efficient and thus can easily surpass one-atom multi-photon absorption [14, 26]. At very high power density ($>10^{11}$ W cm^{-2}, depending on the system), an unusual form of multiply-excited, but rather cold, plasma-like state forms which is expected to autoionize on the time scale of fs to ps.

The first evidence for such a resonant decay process was reported already more than a decade ago, although the exact character of the process was not recognized at that time [27]. In the course of further studies of ICD processes stimulated by the work of Kuleff *et al* [14], such an ionization process was recently studied in Ne clusters [28, 29].

Subsequent experimental work on helium (He) nanodroplets showed clear evidence for a resonant ICD process and a strong enhancement of ionization rates upon resonant excitation of the nanodroplets with respect to direct ionization [26, 30]. This was explained by an ultrafast collective autoionization process (CAI) related to ICD, where several electronically excited atoms are involved (see figures 1(b)–(d)). This process was identified through electron spectroscopy [26], where the dynamics of He nanodroplets resonantly excited to the 1s2p atomic-like states [31] was investigated by intense femtosecond XUV pulses. The electron spectra revealed that in this case, a high-density nanoplasma with a large number of electrons in bound excited states is formed. The novel ionization mechanism is characterized by fast energy or charge exchange and subsequent autoionization of at least three electrons in excited states [26], as depicted in figures 1(b)–(d). In further experiments on Ne clusters, the effect of cascades on ICD was investigated [32]. In these studies, both in Ne and He clusters, however, many questions still remain open, especially pertaining to the transition from two-body ICD to complex many-body autoionization.

Therefore, further detailed studies using simple model systems can add knowledge to the fundamental understanding of such diverse decay processes. He droplets are a unique medium to study interatomic ionization mechanisms due to (i) their simple electronic structure, which leads to few, well-separated spectral lines, (ii) the extremely weak interatomic van der Waals interactions [33, 34], and (iii) the homogeneous, superfluid density distribution, which is nearly independent of the droplet size [35].

In the current study, we address the autoionization dynamics focusing on the transition from two-body ICD to complex many-body autoionization, i.e. CAI. We present a detailed investigation of photoelectron spectra as a function of droplet size and power density. Additionally, through a numerical simulation, we give a thorough explanation of the observed processes. The article is organized as follows. In section 2, we briefly describe the experimental setup. Section 3 starts with an overview of the experimental results and a comparison between direct photoemission and autoionization following resonant excitation. The theoretical model based on a system of rate equations is the subject of section 3.2. The comparison between experimental results and simulation follows in section 4. In the last section 5, the conclusions and outlook are given. Further information is collected in the appendix.

2. Experimental procedure

The experiment was performed at the low density matter (LDM) beam line [36] of the FERMI FEL [3]. XUV pulses with photon energies in the energy range 19–45 eV having a wide range of pulse energies (0.2–30 μJ) were focused by a Kirkpatrick–Baez optical system [37] to a spot size of around 300 μm (FWHM) diameter for photon energies $h\nu$ below the first ionization potential (E_{IP}) of He atom, and to 20 μm (FWHM) diameter for $h\nu > E_{IP}$, respectively. The FEL polarization was chosen to be linear and the polarization axis to be perpendicular with respect to the spectrometer axis, while the estimated pulse length is 130 fs (FWHM). Taking into account the estimated transmission of all optical components of the beamline (∼38%), the power density in the interaction region is calculated to be in the 10^9–10^{12} W cm^{-2} range. For the low power densities the FEL intensity is reduced by using a gas cell attenuator [38].The content of second order radiation in the FEL beam is on the order of a few percent. It gives rise to sharp photoemission lines as measured when the first harmonic is tuned to 43.0 eV. These lines can be easily distinguished from other processes. Since the ICD process is more efficient than direct photoionization with the first harmonic at 43.0 eV (the absorption cross section at 43.0 eV is much smaller than at 21.5 eV), the

contribution of the second harmonic is negligible for He nanodroplets where ICD processes are very efficient. For large nanodroplets and high power density a second harmonic line is not visible and does not play a significant role for resonant excitation at 21.5 eV.

He nanodroplets with an average number of atoms from 250 up to 10^6 were produced in a supersonic expansion of He gas at 50–80 bar stagnation pressure through the conical nozzle (100 μm diameter, half-opening angle of 45°) cooled to a temperature of 28–5 K with a precision of $\pm$0.1 K. The sizes of medium-sized and large He nanodroplets are determined based on titration measurements performed separately [39]. For small He nanodroplets, we used scaling laws [40, 41] and tabulated values for characteristic properties of rare gases [33].

The kinetic energy distributions of emitted electrons were measured using a velocity map imaging (VMI) spectrometer and reconstructed using the pBasex method introduced by Garcia *et al* [42], taking into account the calibration curve of the VMI spectrometer. The resolving power of the spectrometer $\Delta E/E$, was determined to be less than 4% for electron kinetic energies above 10 eV and less than 12% for energies below 10 eV.

3. Results and discussion

3.1. Overview

We start with an overview which is intended to demonstrate how the ionization due to ICD and CAI processes differs from 'conventional', direct photoionization. For reference, experimental photoelectron spectra for direct photoionization of He nanodroplets at $h\nu = 43.0$ eV ($>E_{IP} = 24.59$ eV) are given in figure 2 (left column) for various power densities. The photoline at around 17.0 eV is clearly visible and broadens with increasing power density when many photons are absorbed by the cluster and thus multiple electrons are emitted. This behaviour is generally observed and well-understood [11, 43, 44]. With increasing power density, the droplet charges up resulting in the outgoing electrons having to overcome a deeper Coulomb potential. This results in a shift of the photoline and a broadening of the spectrum due to the contribution of many electrons [11, 43, 44] (details are given in section 3.2.1).

At the highest power density ($>8 \times 10^{12}$ W cm^{-2}), a characteristic plateau in the electron emission spectra is formed which shifts down to lower kinetic energies due to the cluster Coulomb potential build-up [11, 44]. Then, a second maximum is observed around 0 eV which exponentially decays towards increasing electron energies. This feature is indicative of inelastic electron collisions and of evaporative electron emission from a nanoplasma [43, 44].

Figure 2, right column, shows for comparison electron spectra recorded after resonant absorption of two photons at low power density (5×10^9 W cm^{-2}) and multiple photons at high power density 8×10^{12} W cm^{-2}, at the maximum of the 1s-2p band (21.5 eV) of large He nanodroplets. We note that the energy deposited into the nanodroplet after absorption of two 21.5 eV photons equals that of one photon absorption at 43.0 eV. Indeed, at low power density the photoelectron spectra look quite similar. When increasing the power density, however, drastic changes emerge. While the *direct* photoline—as explained above—only broadens towards lower energies, the autoionization spectrum completely changes its shape at high power density.

The peak at ~16 eV vanishes and a broad continuum develops which shifts towards lower energies. The rather narrow peak is due to ICD-like autoionization. In our previous publications [26, 30], we showed that these autoionization processes are extremely efficient, which is a clear indication that the excitations are initially delocalized and during the lifetime of the excited states, the two excited atoms come into direct contact. The very different shape of the autoionization spectra compared to direct ionization at high power density (figure 3(a)) is due to the large number of inelastic collisions of the autoionized electrons with surrounding He atoms in the 2p excited state, resulting in additional loss of kinetic energy by autoionized electrons. The cross section for such inelastic collisions between autoionized electrons, i.e. 'quasi free' electrons within He nanodroplets, with 2p excited atoms is very large (several thousand Mb) and thus the photoline completely vanishes at high power density.

In contrast to direct photoemission, the autoionization electron spectra sensitively depend on the droplet size (see figure 3). For small clusters, the photoline is split into several components (see figure 3(c) and section 4.1 for more details). In larger clusters ($N > 1000$), electron spectra recorded following resonant excitation are almost independent of the excitation energy, because fast relaxation takes place resulting in efficient population of the low lying states (see section 3.2.2).

To summarize, the electron spectra of pure He nanodroplets due to autoionization reflect a complicated dynamics which depends on photon energy, power density as well as droplet size. In particular, for resonant excitation, a transition from two-body ICD to collective many-body autoionization is observed for increasing XUV power density and He droplet size.

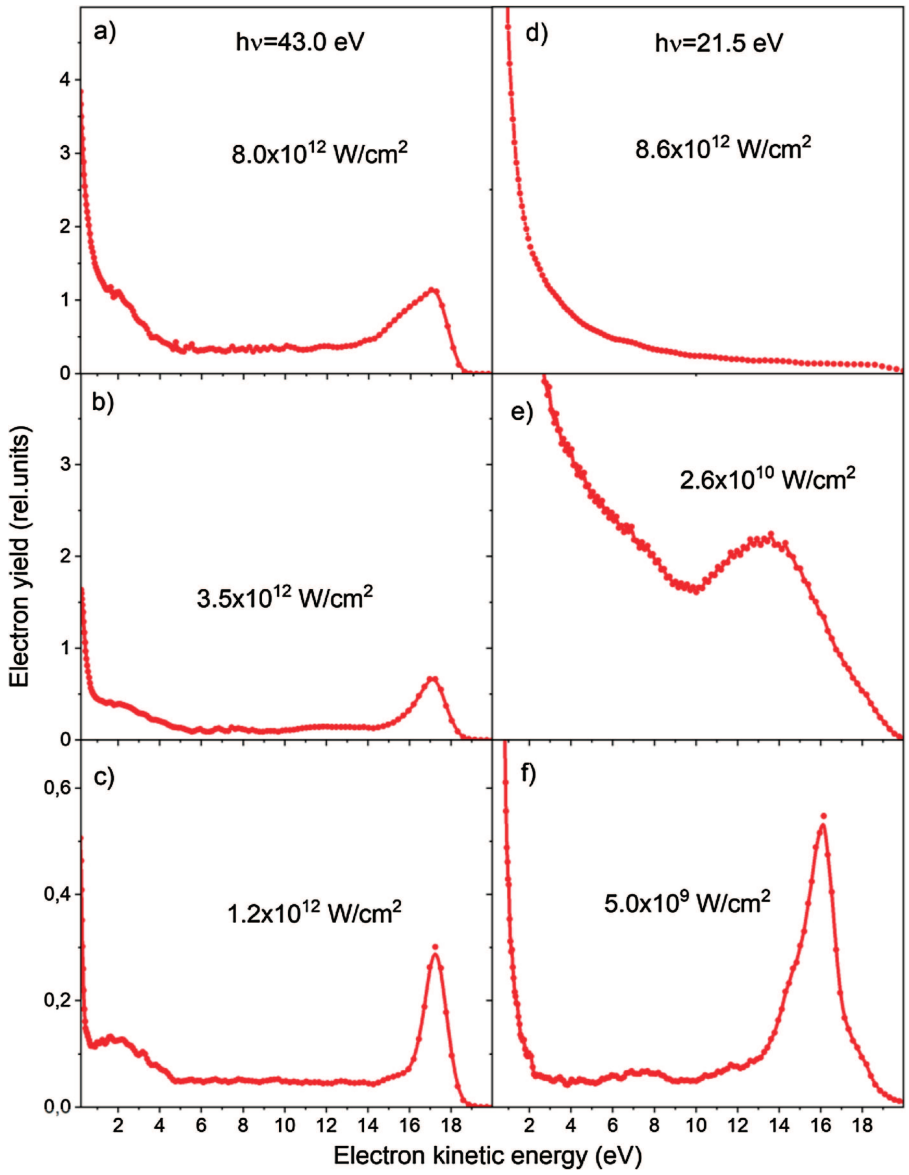

Figure 2. Electron spectra of large He nanodroplets (mean droplet size $\langle N \rangle = 50\,000$) at different power densities: left-hand side [(a)–(c)]—direct photoemission at 43.0 eV photon energy; right-hand side [(d)–(f)]—autoionization spectra due to resonant absorption of few photons of 21.5 eV at 5×10^9 W cm^{-2} (ICD) to multi-photon absorption at 8×10^{12} W cm^{-2} (CAI). For details, see text.

3.2. Details of the model and numerical simulation

To extract more quantitative and systematic information from the measured data, we have developed a simple numerical model to compare with the experimental spectra. The full dynamics of the ICD and CAI processes induced in He nanodroplets by resonant excitation of 1s2p atomic-like states by intense XUV laser fields ideally should be simulated using a quantum mechanical description, which unfortunately cannot currently be achieved. Instead, semi-classical approaches are widely used to model interaction processes in clusters [45, 46]. These are based on the description of the atomic ionization processes via suitable rates, whereas the dynamics of the resulting ions and electrons are treated by classical dynamics [44]. Unfortunately, this approach is difficult to apply to resonantly excited He nanodroplets because of the contribution of several processes and their interrelations. Therefore, at present, our experimental results can only be treated by numerical simulations based on a set of rate equations. By using the Monte-Carlo method, various processes can be taken into account, such as multi-step ionization [10, 43], interatomic Coulombic decay [14], secondary inelastic collisions [10, 26], and desorption of electronically excited atoms in He droplets [47], as well as ultrafast electronic relaxation and CAI processes.

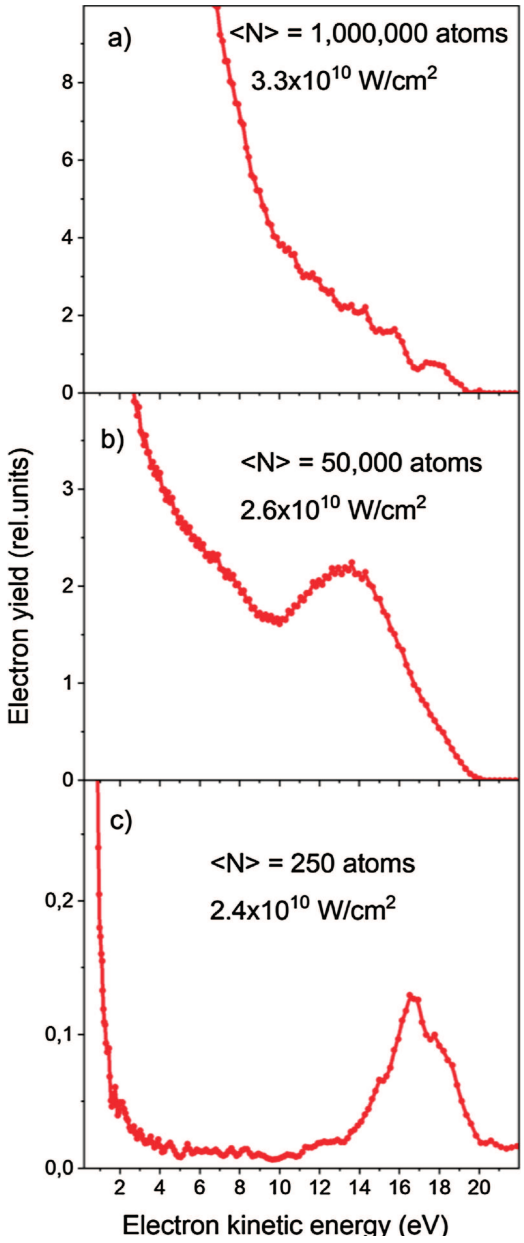

Figure 3. Electron spectra for resonant excitation at 21.5 eV photon energy and $\sim 3 \times 10^{10}$ W cm^{-2} power density for different He nanodroplet sizes: (a)—He nanodroplet with $\langle N \rangle = 1000\,000$ atoms; (b)—He nanodroplet with $\langle N \rangle = 50\,000$ atoms; (c)—He nanodroplet with $\langle N \rangle = 250$ atoms.

3.2.1. Line broadening and shifts due to multi-step ionization

As already mentioned in the previous section, at a photon energy well above the first ionization energy E_{IP}, photoelectron spectra can be interpreted by a sequence of direct electron emission events in the developing Coulomb field [14] called multi-step ionization [11, 43]. While the droplet absorbs many photons, electrons are ejected one after another thereby charging up the droplet. As a result, electrons emitted at later stages need to overcome the Coulomb potential created by the charged droplet and thus lose part of their kinetic energy [11, 43]. Here the escape of electrons is described as an instantaneous process, i.e., the emitted electrons leave the droplet before the next ionization event occurs, thereby neglecting any further energy exchange. Assuming the droplet ionization process is a series of instantaneous electron emission events due to direct photoemission from the developing droplet Coulomb field and accepting that the ionization events are counted only if the single-particle energy of the released electron is positive, the asymptotic kinetic energy of an electron released from the jth ion is determined by [11, 43]

$$E_j = h\nu - E_{\mathrm{IP}} - \frac{e^2}{4\pi\varepsilon_o}\sum_{i\neq j}\frac{q_i}{r_{ij}}, \tag{2}$$

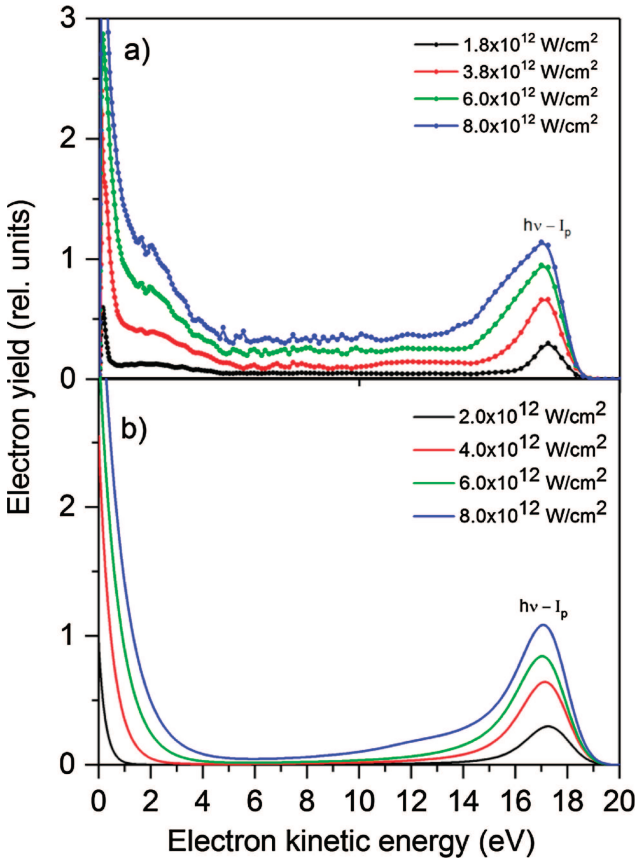

Figure 4. Electron spectra of He nanodroplets irradiated at 43.0 eV photon energy and different power densities: (a) experimental results for He droplet of $\langle N \rangle = 50\,000$ atoms, (b) simulations for He droplet of $N = 50\,000$ atoms.

where $h\nu$ is the photon energy, E_{IP} is the ionization potential and i runs over all other ions with charge state q_i (integer number) and distance between electron and ions, r_{ij}. The last term in equation (2) describes the Coulomb downshift due to the previously generated ions with charge states q_i (in our case $q_i = 1$) at positions r_i. In this way, Monte Carlo simulations of the photoelectron spectra can be performed, where only direct ionization events, i.e., electrons with total energy >0, are considered. At sufficiently high power density, the emission process stops since the electrons cannot escape from the deep Coulomb potential of the droplet and the electron emission becomes frustrated [11].

Electron spectra of He nanodroplets of size 50 000 atoms were measured in the regime of direct photoionization at $h\nu = 43$ eV for different laser intensities (see figure 4(a)). At increasing intensity, the photoline at 17 eV broadens towards lower electron energies and an extended wing reaching down to zero energy appears. These features are indicative of multi-step photoionization of clusters and nanodroplets [11, 44]. The narrow low-energy feature results from evaporative electron emission out of a nanoplasma formed by collective autoionization of the multiply excited nanodroplets [26]. The corresponding simulated spectra are shown in figure 4(b).

They reproduce all the characteristic spectral features quite well. Thus, we conclude that He nanodroplets irradiated at $h\nu > E_{IP}$ follow similar photoionization dynamics as small heavier rare-gas clusters, which feature a characteristic plateau in the photoelectron spectrum [11, 43]. Electrons released by autoionization should be affected in the same way by the developing Coulomb potential as photoelectrons. Therefore, the effect of multi-step ionization—broadening of photolines and the formation of a plateau—is also taken into account in our simulations for $h\nu < E_{IP}$.

3.2.2. Resonant excitation and the role of excited states

For the case of resonant excitation ($h\nu = 21.5$ eV), electrons can only be emitted by two-photon ionization or by autoionization due to ICD-like processes [14]. Considering that the photoionization cross sections of He excited (He^*) states (2^1S, 2^3S, 2^1P) are less than 0.05 Mb [48], and the power density of the FEL beam is below 10^{11} W cm^{-2}, conventional two-photon ionization is not expected to significantly contribute to the ionization signals and is therefore neglected in our model, see also reference [14]. As shown in reference [30], the fraction of He nanodroplets ionized by sequential two-photon ionization at $h\nu = 21.5$ eV and

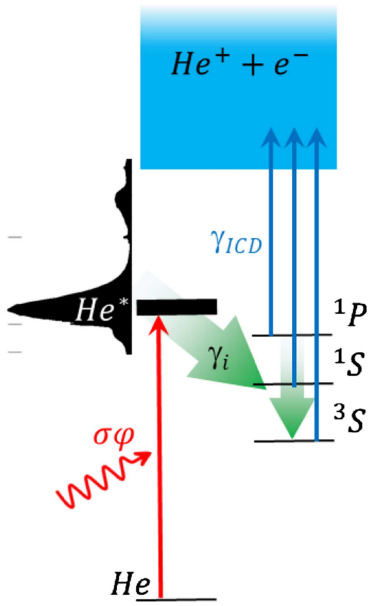

Figure 5. Schematic representation of possible decay channels of excited He nanodroplets at 21.5 eV photon energy. The He nanodroplet photoabsorption spectrum is indicated in black [31]. After irradiation of He nanodroplets at 21.5 eV, excited He droplet states can relax to low lying 2s and 2p atomic excited states (green arrows, →). Then, if a second photon is absorbed and two excitations come into close contact, autoionization by ICD can occur in the course of the relaxation (blue arrows, →). For details see text.

power density of 10^{13} W cm^{-2} is expected to be only 0.6%. Stimulated emission is neglected because of efficient depletion of He* states via ICD. Thus, in our model for multiply excited He nanodroplets, we assume ICD to be the primary ionization process which we refer to as multi-step ICD. Since the ICD mechanism is expected to be very efficient [13], we assume that *every* pair of He droplet excited states will undergo ICD producing one ionized and one neutral atom.

Furthermore, fast electronic relaxation of the He nanodroplet excited states [25, 49] to low-lying 2^1S, 2^3S, 2^1P atomic excited states has been reported in the work of Mudrich *et al* [50]. It shows that the band-excited state in He nanodroplets decays to the atomic 1s2p and 1s2s states within hundreds of fs. Thus, 1s2p (^{1}P$_1$) → 1s2s (^{1}S$_o$) relaxation takes place followed by slow 1s2s (^{1}S$_o$) → 1s2s (^{3}S$_1$) relaxation (ns time scale) [50]. Ultrafast electronic relaxation was also found for Ne and Xe clusters [51, 52]. Various important relaxation processes in He nanodroplets are schematically depicted in figure 5.

In the beginning, 2p droplet excited states denoted by He* undergo ultrafast relaxation to the atomic 1s2p ^{1}P, 1s2s ^{1}S and 1s2s ^{3}S states with the relaxation rate constants γ_i followed by ICD between pairs of these states at the decay rate constant γ_{ICD} (see equation (3)). Based on our experimental findings (see section 4.1, figure 7), we assume that ICD occurs between 1s2s ^{3}S, 1s2s ^{1}S and 1s2p ^{1}P pairs of identical excited states within a droplet while we detect no significant contribution of intercombination bands. In other words, 2s–2p interactions are not observed or at least are at the noise level of our experimental results. The contribution of ^{3}S and ^{1}S states as well as the absence of intercombination bands, such as 2p–2s, provides information about the character of the ICD process [14, 24]. In particular, the prominent contributions of the metastable states ^{3}S and ^{1}S to the ICD signal indicates that ICD predominantly proceeds by charge exchange whereas the virtual photon process [14] is less important. A similar conclusion was recently drawn for the system He* + M, where M stands for an alkali metal atom [25]. This is due to the diffuse structure of the electron orbitals of both the alkali metal atom and the He* atom.

3.2.3. Numerical model

Based on the processes mentioned above as well as the proposed way of computing the number of excited and ionized states in [14], we model the evolution of excited He droplets by the system of rate equations

$$\dot{N}_0(t) = -\sigma_0 \cdot \varphi(t) \cdot N_0(t) + \dot{N}_i^{\mathrm{ICD}}(t) \tag{3a}$$

$$\dot{N}^*(t) = \sigma_0 \cdot \varphi(t) \cdot N_0(t) - \sum_{i=1}^{3} \gamma_i \cdot N^*(t) \tag{3b}$$

$$\dot{N}_i(t) = \gamma_i \cdot N^*(t) - 2 \cdot \dot{N}_i^{\mathrm{ICD}}(t) \tag{3c}$$

$$\dot{N}_i^{\mathrm{ICD}}(t) = \frac{1}{2} \cdot \gamma_{\mathrm{ICD}} \cdot N_i(t) \tag{3d}$$

Table 1. Numerical factors used in the simulation of the ionization dynamics of 1s2p $^1P_1$ excited He droplets. All time constants are with respect to decay to the 1/e level.

Excitation photon energy, $h\nu$	21.5 eV
FEL pulse width (FWHM), $\Delta\tau$	130 fs
Spectrometer energy resolution, $\Delta E/E$	4%
Gaussian profile of the FEL beam (FWHM)	300 μm
He droplet excitation cross-section per atom [18, 26], σ_o	50 Mb
Electron-impact 2p ionization cross-section [53], $\sigma_{2p\to inf}$	1200 Mb
Electron-impact 2p $\to nl$ excitation cross-section [53], $\sum_{n=3}^{5}\sigma_{2p\to nl}$	2800 Mb
Droplet relaxation time to 1s2p and 1s2s atomic excited states [50]	1–2.5 ps
1s2p ($^1P_1$) $\to$ 1s2s (^1S_o) relaxation time [50]	1 ps
Radiative decay time of 1s2s (^1S_o) and 1s2s ($^3S_1$) atomic excited states	100 ns
ICD decay time (assumption), τ_{ICD}	500 fs
He desorption time [54]	15 ps
Ionization potential, E_{IP}	24.59 eV
Internuclear separation [55]	3.36 A
Simulation time step	1 fs
Number of iterations per step point	10 000
Time interval with respect to the FEL pulse	from −500 fs to +1500 fs

Equation (3a) corresponds to the time evolution of the neutral ground states, where σ_o is the absorption cross section, $\varphi(t)$denotes the photon flux which contains the information about the temporal profile of the pulse and $N_o(t)$ is the number of ground states in the He nanodroplet as a function of time. Equation (3b) corresponds to the time evolution of the droplet excited states $N^*(t)$, where γ_i are the rate constants for relaxation into atomic excited states $i = 2s\ ^3S$, $2s\ ^1S$, $2p\ ^1P$. Equation (3c) corresponds to the time evolution of the atomic excited states for all i, where $\dot{N}_i^{ICD}(t)$ is the ICD rate in state i. The ICD rate is given in equation (3d), where γ_{ICD} is the rate constant for ICD which is assumed to be the same for all atomic states i. The total number of ICD electrons is then given by $\int_0^\infty \dot{N}_i^{ICD}(t)\,dt$.

To simulate the electron spectra, we solve the rate equation model numerically using the Monte-Carlo method. We start the simulation by determining the number of droplet excited states over the whole FEL pulse with a simulation time step of 1 fs, based on the FEL power density, FEL pulse width, and He droplet excitation cross-section per atom σ_o [18, 26]. We randomly distribute the He* states over the nanodroplet. In our simulation, we assume that the initially delocalized excitations come in close contact due to their mutual attraction, at least on the length scale of ~1 nm which is the relevant distance in our present study with power densities of 10^{10} W cm^{-2} and more. Autoionization preferentially takes place between neighbouring excited atoms due to the short-range character of ICD driven by charge exchange [14]. Therefore, the distance-dependence of the ICD rate is not explicitly taken into account. Almost all parameters in the model (see table 1) are known from the literature. Free parameters are the expected ICD rate, which is equal to $1/\tau_{ICD}$ and the droplet relaxation rates to 1s2p and 1s2s atomic excited states [50]. These parameters were adjusted so as to globally maximize the agreement between the simulated and experimental spectra.

For each time step of the simulation, we evaluate the probability of undergoing a discrete relaxation or ICD ionization process. The final electron energies are obtained by summing over the modelled multi-step ionization processes [43] of individual ICD components (based on equation (2)),

$$E_j^{ICD} = 2h\nu - E_{IP} - \frac{e^2}{4\pi\varepsilon_o}\sum_{i\neq j}\frac{q_i}{r_{ij}} \tag{4}$$

Finally, the obtained electron spectra are convoluted by the instrument function of the VMI spectrometer, given by a Gaussian function with relative FWHM of 4% (see table 1). For the resonant-excitation case (21.5 eV), when the FEL beam has 300 μm spot size, the intensity-averaging over the volume of the focus is not taken into account, while for the direct photoionization at $h\nu = 43.0$ eV and 20 μm spot size, this effect is considered. All parameters relevant for the numerical simulation are given in table 1.

As an example, the simulated ionization dynamics of a small He nanodroplet (250 atoms) resonantly excited at $h\nu = 21.5$ eV by a 130 fs FEL pulse with intensity $I = 2.4 \times 10^{10}$ W cm^{-2} is shown in figure 6. When the FEL beam interacts with He nanodroplets, a large number of 2p-excited states N^* are formed resulting in quasi-free electrons in the droplets due to ICD.

As has been shown in reference [10] and reference [26], inelastic electron collisions in this case are very efficient. Therefore, the number of excited He atoms $N_{excit.}(t)$ (see figure 1(d)) and the number of ionized atoms $N_{ioniz.}(t)$ (see figure 1(c)) by inelastic electron collisions as a function of time t is given by

$$\dot{N}_{inel.}(t) = \dot{N}_{excit.}(t) + \dot{N}_{ioniz.}(t), \tag{5a}$$

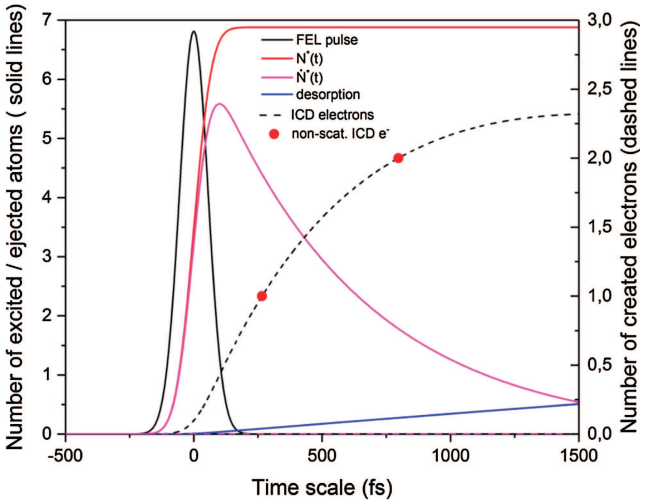

Figure 6. Simulated ionization dynamics of 1s2p $^1P_1$ excited states in He_{250} nanodroplets irradiated by 130 fs FEL pulses (solid black line, –) and at 2.4×10^{10} W cm^{-2} power density. The total number of excited atoms $N^*(t)$ is shown by the solid red (–) line. The evolution of excited states $\dot{N}^*(t)$ due to ICD and desorption solid blue line (–) of the excited atoms is shown by the solid magenta (–) line. The total number of created ICD electrons and the discrete number of non-scattered ICD electrons (non-scat. ICD e$^-$) are shown as a dashed black line (–) and as red dots (•), respectively. For this droplet size and power density the inelastic electron scattering process is negligible.

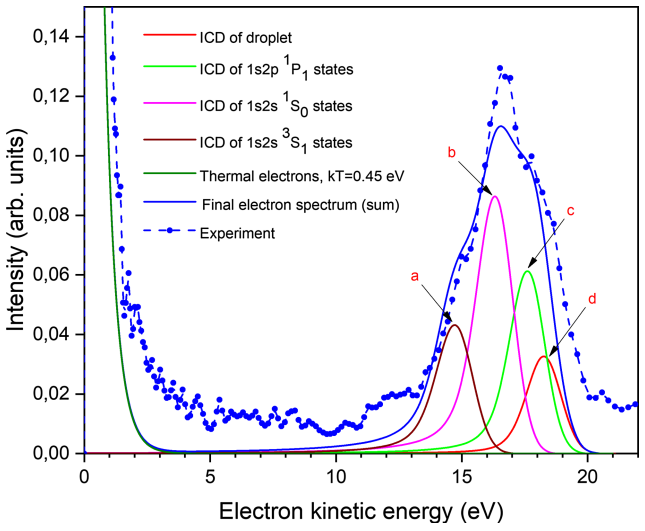

Figure 7. Experimental and simulated electron spectrum of small He nanodroplets ($\langle N \rangle = 250$ atoms) irradiated at $h\nu = 21.5$ eV and $I = 2.4 \times 10^{10}$ W cm^{-2} [solid blue (–) line]. Electron spectra due to ICD of droplet excited states, atomic 1s2p $^1P_1$, 1s2s (^1S_o) and 1s2s ($^3S_1$) states are presented by feature (d), (c), (b) and (a), respectively. The distribution of thermally evaporated electrons with a temperature of 0.45 eV $k_B{}^{-1}$ is represented by the solid dark green (–) line. The sum of all spectra is shown by the solid blue (–) line. The experimental result is given by the dash-dotted blue (–·–) line.

where

$$\dot{N}_{\text{excit.}}(t) = \sum_{i=1}^{3} \sum_{n=3}^{5} k_{i\to nl} \cdot N_i^{\text{ICD}}(t) \cdot N_i(t) \tag{5b}$$

$$\dot{N}_{\text{ioniz.}}(t) = \sum_{i=1}^{3} k_{i\to\text{inf}} \cdot N_i^{\text{ICD}}(t) \cdot N_i(t) \tag{5c}$$

Here, $k_{i\to nl}$ and $k_{i\to\text{inf}}$ are the rate constants for the electron-impact excitation and electron-impact ionization of the He atom from the i-excited state to high lying nl levels and to the continuum, respectively. Equation (5b) contains the sum of $k_{2p\to nl}$ rate constants, where the principal quantum number n runs over the states whose contributions to the total cross section is largest ($n = 3$–5).

Another important relaxation process, which also has to be considered, is the desorption of electronically excited atoms and molecules from He droplets [47, 56]. As was discussed in reference [47], excited atoms He^* and molecules (excimers) He_2^* tend to form void bubbles around themselves due to Pauli repulsion between the outer electron and the surrounding He. The bubble states can freely move to the surface where the He^* and He_2^* are ejected into vacuum [57]. Since the electronically excited molecules desorbing from the droplet are far from being thermalized, the coupling between the electronically excited molecule and the droplet is very weak. Therefore, we assume that the excited species leave the droplet in a very short time [49, 56]. This effect is taken into account by adding the term to equation (3b)

$$\dot{N}_{\mathrm{des}}(t) = \gamma_{\mathrm{des}} \cdot N^*(t) \tag{6}$$

where γ_{des} is the desorption rate constant.

In this way, electron spectra of He nanodroplets where inelastic electron collisions play a role have been modelled using the rate equation system (3) which is amended by additional terms for both inelastic scattering and desorption. As an example, the simulated ionization dynamics of He nanodroplets (50 000 atoms) irradiated at $h\nu = 21.5$ eV by 130 fs FEL pulses at $I = 2.4 \times 10^{10}$ W cm^{-2} is shown in the appendix, see figure A1. For the case of large He nanodroplets, (see section 4.3), the ICD electron can scatter several times within a droplet thereby losing part or all of its energy in each collision. If more than two particles are involved in the process, CAI [26, 30] takes place.

4. Comparison between experimental results and simulations

In the following we present both experimental and numerical results for the resonant excitation of He nanodroplets irradiated at $h\nu = 21.5$ eV by 130 fs pulses in the 10^{10}–10^{11} W cm^{-2} power density range. To obtain sufficient statistics, the experimental results have been averaged over 3000 shots and ensemble averaging over 10^5 simulations was performed.

4.1. ICD in small He droplets

To provide a basis for the forthcoming discussions, we start our analysis from the simplest case, i.e., small He nanodroplets (~250 atoms/droplet) resonantly irradiated at $h\nu = 21.5$ eV and relatively low power densities. At these experimental conditions, electrons can leave the He droplets due to ICD. The electron spectra of He droplets irradiated at $h\nu = 21.5$ eV and $I = 2.4 \times 10^{10}$ W cm^{-2} are simulated by modelling the time evolution of the excited He nanodroplets (see figure 6, section 3.2.3) up to 1.5 ps.

Detailed information about the ionization mechanisms and dynamics can be inferred from figure 7. The ICD path through the 1s2s ^1S_o state gives the largest contribution to the final electron spectrum which can be explained by the ultrafast relaxation of the 1s2p ($^1P_1$) state to the 1s2s (^1S_o) state and subsequent slow 1s2s (^1S_o) → 1s2s ($^3S_1$) relaxation (see section 3). The sum of electron spectra from different excited states is shown by the solid blue (–) line in figure 7 while the dash-dotted blue (–·–) line shows the experimental result at $I = 2.4 \times 10^{10}$ W cm^{-2}. Good agreement between experimental data and numerical simulations is achieved when assuming an ICD rate constant of 1/(500 fs) for all excited states. This value matches the results in [50].

The low kinetic energy component of the electron distributions is attributed to thermal evaporation of electrons out of the nanoplasma induced by collisional equilibration of quasi-free electrons [11, 27]. This component is implemented in the simulated electron spectrum by adding an exponential decay fit function obtained from the experimental results (see figure A3 in appendix), from which we infer an electron temperature of about 0.45 eV k_B^{-1}.

As seen from the experimental results (figure 7), the electron spectra are rather complicated and do not show a single line as predicted by the pure ICD model [14]. Instead, there are several overlapping peaks which are assigned to ICD of pairs of 1s2s ^3S, 1s2s ^1S and 1s2p ^1P atomic states [18] within a droplet, labelled as 'a', 'b' and 'c', respectively:

$$\begin{aligned}
&(\mathrm{a})\mathrm{He}^*(1s2s\,^3S) + \mathrm{He}^*(1s2s\,^3S) \rightarrow \mathrm{He}(1s^2) + \mathrm{He}^+(1s) + e_1(15.08\ \mathrm{eV})\\
&(\mathrm{b})\mathrm{He}^*(1s2s\,^1S) + \mathrm{He}^*(1s2s\,^1S) \rightarrow \mathrm{He}(1s^2) + \mathrm{He}^+(1s) + e_2(16.68\ \mathrm{eV})\\
&(\mathrm{c})\mathrm{He}^*(1s2p\,^1P) + \mathrm{He}^*(1s2p\,^1P) \rightarrow \mathrm{He}(1s^2) + \mathrm{He}^+(1s) + e_3(17.88\ \mathrm{eV})
\end{aligned} \tag{7}$$

The kinetic energy of the ICD electron is given by $E_e = 2 \times E(\mathrm{He}^*) - E_{IP}$, where $E(\mathrm{He}^*)$ is the energy of the excited level of He^* and E_{IP} is the ionization potential of He atoms. The influence of the He droplet on the energetics of the ICD is neglected owing to the weak coupling of the excited and ionized atoms to the He droplet surface. The emission of ICD electrons from low-lying atomic excited states gives clear evidence

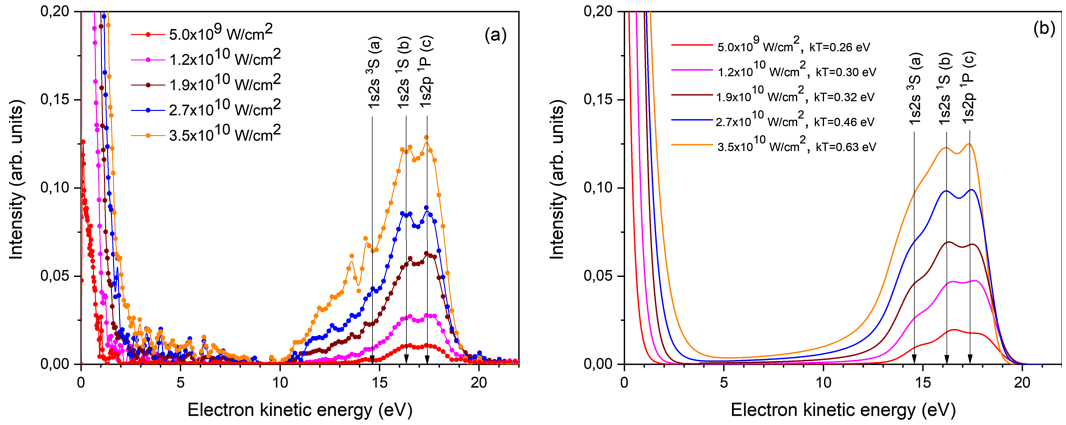

Figure 8. Electron spectra of medium sized He droplets irradiated at $h\nu = 21.5$ eV and low power densities: (a) experimental results for He droplet size of $\langle N \rangle = 1000$ atoms; (b) numerical simulations for He droplet size of $N = 1000$ atoms. Maxima (a), (b) and (c) correspond to ICD of pairs of 1s2s ^{3}S, 1s2s ^{1}S and 1s2p ^{1}P atomic states [18] within a droplet, respectively.

for ultrafast (hundreds of fs) electronic relaxation. This is in good agreement with our recent experimental results on He nanodroplets [50]. Feature 'd' at 18.43 eV is caused by ICD of droplet excited states as well as by direct photoionization of He nanodroplets or surrounding He atoms from the FEL second harmonic radiation (estimated to be less than 1% of the total signal). All in all, the experimental results and our model are in reasonable agreement.

4.2. ICD in medium-sized He nanodroplets

Experimental electron spectra of medium-sized He nanodroplets (∼1000 atoms) irradiated at $h\nu = 21.5$ eV are shown in figure 8(a). Under these conditions the structure of the electron spectrum becomes broader. Despite the fact that the features around 14.6 eV, 16.3 eV and 17.4 eV are less pronounced compared to small He droplets, they are assigned to ICD of pairs of 1s2s ^{3}S, 1s2s ^{1}S and 1s2p ^{1}P atomic states [18] within a droplet, correspondingly. The same model as for the small He droplets (see section 3.2.3) was used for simulating the electron spectra for medium sized He droplets (see figure 8(b)).

Based on our numerical simulations and especially on the fact that the same model provides good agreement between experimental and simulated results for two different droplet sizes, we conclude that the decay pathways for He_{1000} nanodroplets are essentially the same as for He_{250} nanodroplets. The broadening of electron spectra is mainly caused by an increasing number of unscattered electrons, which then play a role in the multi-step ICD electron emission. Under these experimental conditions inelastic electron scattering is negligible.

Increasing the number of atoms within the He nanodroplet up to 2500 atoms leads to further broadening of the spectral features (see figure 9) due to the creation of a larger number of unscattered ICD electrons. As a consequence, the spectral components from different states merge to one broad peak, which shifts toward lower kinetic energies when increasing the power density, see figure 9.

In contrast to the small He nanodroplets, it becomes difficult to unambiguously assign the various decay channels and their contributions to the electron spectra. Nevertheless, our model still nicely reproduces the experimental electron spectra for resonantly excited He nanodroplets of 2500 atoms. There are some deviations between experimental and simulated main peak widths for the low power densities ($I \sim 10^{10}$ W cm^{-2}), but the overall behaviour remains consistent. The broadening of the maxima in the numerical simulations can be explained by the fixed values of the decay rates in the simulation. In reality, we expect that these values slightly vary depending on both droplet size and power density.

Our simulation shows that even at $I = 1.5 \times 10^{11}$ W cm^{-2}, inelastic electron scattering plays only a minor role for medium-sized He nanodroplets. Nevertheless, the structure of the electron spectra is drastically blurred by the large number of quasi-free electrons in collisional equilibrium [11, 43], which leads to thermal electron emission [44]. Moreover, at higher power density, it clearly shows a transition from ICD-type autoionization to CAI, see figure 1(b). The corresponding electron spectral component, from which we infer an electron temperature in the range of 0.3–3.3 eV k_B^{-1}, is included in the simulation results, see figure 9(b).

4.3. ICD in large He nanodroplets

Resonant excitation of large He nanodroplets, for the case that the number of atoms per droplet exceeds 50 000 atoms, leads to additional structures and broadening of the electron spectra, see figure 10. As

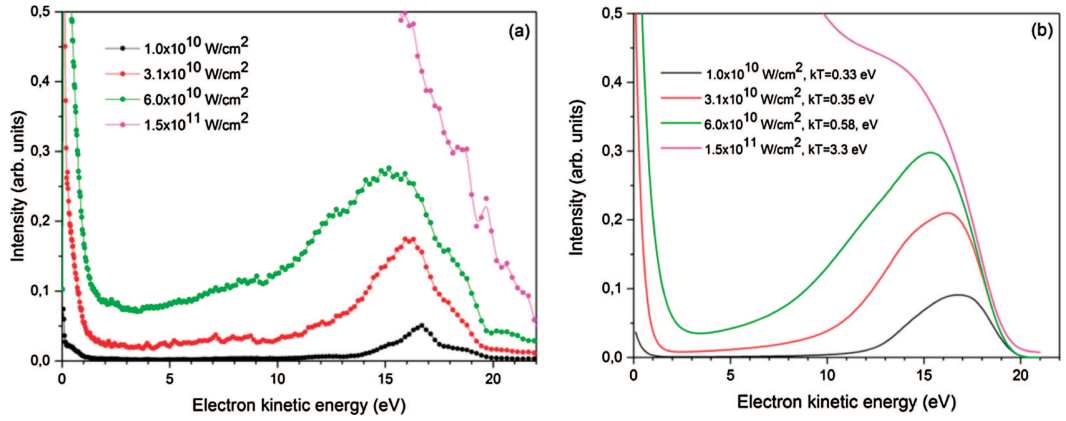

Figure 9. Electron spectra of medium-size He droplets irradiated at $h\nu = 21.5$ eV and low power densities: (a) experimental results for He droplets composed of $\langle N \rangle = 2500$ atoms; (b) numerical simulations for He droplet size of $N = 2500$ atoms.

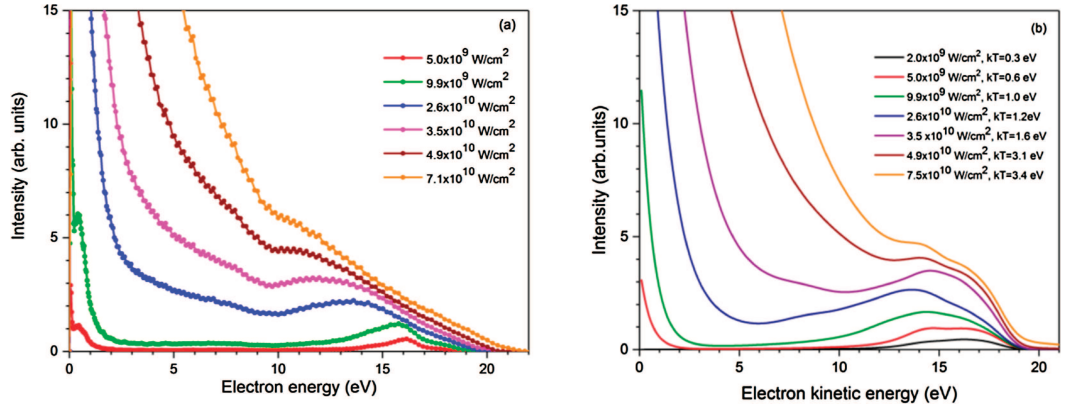

Figure 10. Electron spectra of large He droplets irradiated at $h\nu = 21.5$ eV and low power densities: (a) experimental results for He droplet size of $\langle N \rangle = 50\,000$ atoms; (b) numerical simulations for He droplet size of $N = 50\,000$ atoms.

mentioned in section 3, ICD electrons can scatter several times within a droplet, thereby losing part of their energy. Additionally, when more than two electronically excited atoms are involved, a transition from ICD to CAI [26, 30] takes place. This transition is controlled by the number of excited He atoms per He nanodroplet and occurs at about 1200 He^* per droplet.

For example, already at $I = 2.6 \times 10^{10}$ W cm^{-2} [see figure 10(a), dotted blue (–·–) line] a sufficiently large number of ICD electrons can scatter on 2p excited atoms within $He_{50\,000}$ nanodroplets (see simulations for the atomic 1s2p $^1P_1$ excited states in appendix, figure A1), and further excite the atoms to high-lying *nl* excited states. A similar behaviour is seen for 1s2s ^{3}S, 1s2s ^{1}S atomic excited states and droplet excited states. As a result, ICD-created electrons from all atomic excited states lose energy due to scattering leading to additional structures in the electron spectra. Additionally, the electron spectra of the individual components are strongly broadened due to multi-step ICD electron emission [11, 43]. A further increase of the power density in $He_{50\,000}$ nanodroplets even leads to multiple scattering events, see figure A2 in the appendix.

As seen in figure 10, there is good agreement between experimental and simulated results even in this multiple scattering regime. Our experimental and simulation results clearly show that the photoline is almost quenched, many excited atoms contribute and CAI [26, 30] and thermal electron emission provide the main contributions to the electron spectra. Thus, CAI starts to play a significant role already at 2.4×10^{10} W cm^{-2} power density for $He_{50\,000}$ nanodroplets, where many electron scattering events become possible, see figure A1 in the appendix. With increase of the power density to 7.5×10^{10} W cm^{-2}, the number of scattering events increases dramatically, see figure A2 in the appendix, nanoplasma formation becomes possible and the primary contribution to the electron spectra stems from nanoplasma electrons, see figure 11.

A large fraction of created electrons in a broad energy range at some point cannot overcome the Coulomb barrier, which leads to the frustration of multi-step ICD electron emission [43]. Thereby the

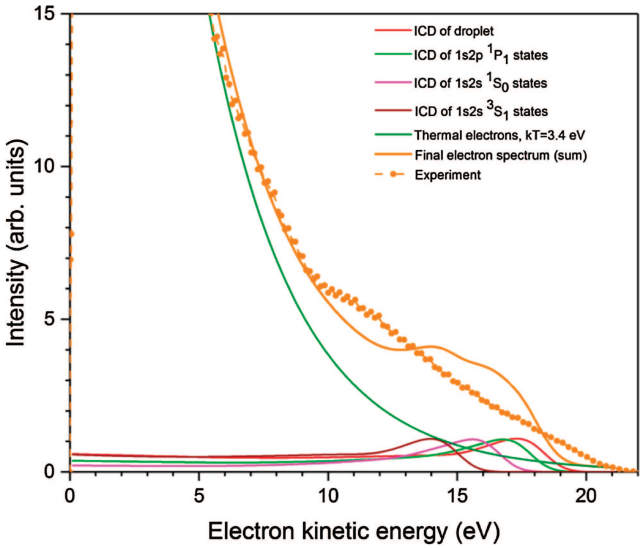

Figure 11. Simulated electron spectra of large He nanodroplets ($N = 50\,000$ atoms) irradiated at $h\nu = 21.5$ eV and $I = 7.5 \times 10^{10}$ W cm^{-2} [solid orange (–) line in figure 10(b)]. Electron spectra from ICD of droplet exited states and atomic 1s2p $^1P_1$, 1s2s (^1S_o) and 1s2s ($^3S_1$) states are presented by solid red (–), solid green (–), solid magenta (–) and solid brown (–) lines, respectively. Thermal electron evaporation at the electron temperature of 3.4 eV $k_B{}^{-1}$ is given by the solid dark green (–) line. The sum of all spectra is shown by the solid orange (–) line. The experimental result from figure 11(a) is given by the dotted orange (–·–) line.

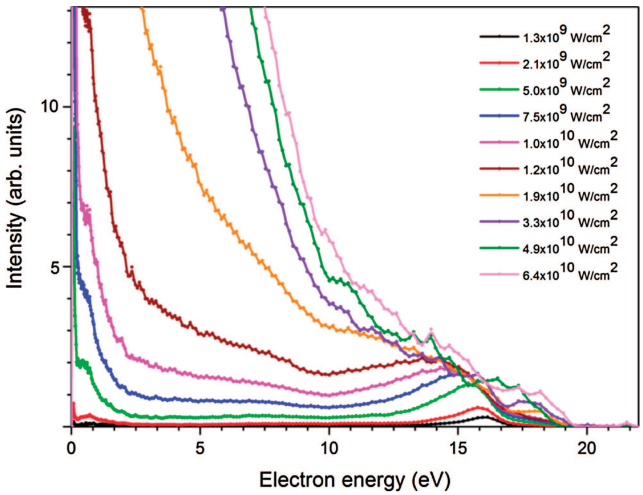

Figure 12. Measured electron spectra of extremely large He nanodroplets ($\langle N \rangle = 10^6$ atoms) irradiated at $h\nu = 21.5$ eV and low power density.

quasi-free electrons are trapped in He nanodroplets leading to the formation of a cold nanoplasma and to the evaporative emission of thermal electrons. Similar to the case of small He droplets, the contribution of the nanoplasma electrons is taken into account by an exponential function fitted to the experimental results with an electron temperature of 3.4 eV $k_B{}^{-1}$.

When increasing the number of atoms in He nanodroplets up to 10^6, the general structure of the electron spectra does not change much (see figure 12). Here, thermal electron emission out of a nanoplasma plays the main role even at lower power densities. Additionally, as shown in reference [26], a high-density plasma with broad electron features can be formed due to the fact that more than three or four excited atoms are in direct contact (see figure 1(b)), leading to the formation of a continuous network of excited states, i.e., when the excitation probability approaches a critical value of electronically excited atoms [26]. In our previous work [26] we estimated that if more than 12% of the atoms in the droplet are excited, such a network will form at the expense of interacting dimers, trimers, and larger isolated oligomers [58]. For these conditions, the ICD lines get completely quenched (see figures 2(d–e) and 12), because a large

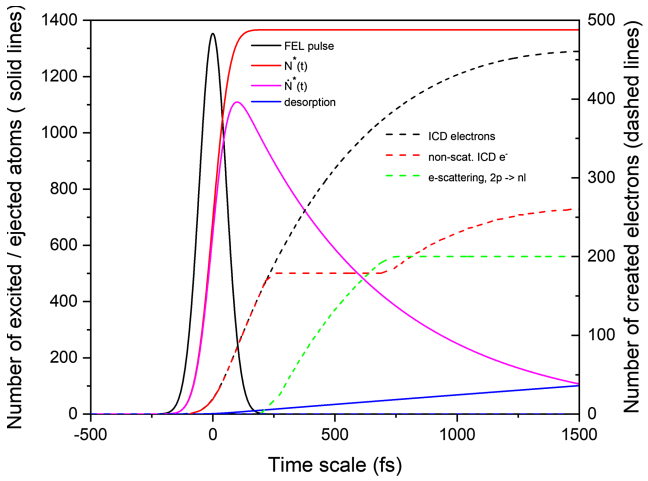

Figure A1. Simulated ionization dynamics of 1s2p $^1P_1$ excited states within $He_{50\,000}$ nanodroplets by 130 fs FEL pulses solid black line (–) at 2.4×10^{10} W cm^{-2} power density. The total number of excited atoms $N^*(t)$ is shown by the solid red (–) line. The evolution of excited states $\dot{N}^*(t)$ due to both ICD decay and desorption (solid blue line (–)) of the excited atoms is given by the solid magenta (–) line. The total number of created ICD electrons and the discrete number of non-scattered ICD electrons (non-scat. ICD e$^-$) are shown by the dashed black (--) and dashed red (--) lines, respectively. Inelastic electron-impact excitation of 2p excited states to high-lying *nl* levels (e-scattering, 2p $\rightarrow$ *nl*) is shown by the dashed green (--) line, respectively.

number of electronically excited atoms are created inside the nanodroplet before autoionization by ICD of two excited atoms takes place. Furthermore, the observation that quenching of the ICD line comes about at rather modest power density of $\sim 10^{10}$ W cm^{-2} (see figure 12), much lower than for small clusters ($N \sim 200$), is a strong indication that the whole dynamics is governed by the number of excited atoms inside the cluster rather than by their density. In other words, the distance between initially excited atoms does not play such a strong role as might be expected from the steep distance dependence of the ICD rate for isolated pairs of atoms, since the excitations are delocalized and always 'find' each other. Modelling this regime is beyond the scope of the present manuscript, but should trigger more thorough theoretical studies of the dynamics of cluster and nanodroplet autoionization.

5. Summary and conclusions

The ionization dynamics of He nanodroplets resonantly excited to the 1s2p band-like state at 21.5 eV photon energy by intense femtosecond XUV pulses in the range of power densities 10^9–10^{12} W cm^{-2} have been investigated by photoelectron spectroscopy. Our experimental results are interpreted with the aid of Monte Carlo simulations based on a simplified rate equation model including various processes such as multi-step ionization [10, 43], ICD [14], secondary inelastic collisions [10, 26] and desorption of electronically excited atoms from He droplets [47], as well as electronic relaxation processes. The complex dynamics depend sensitively on droplet size and XUV power density.

In small droplets the resonantly excited He-droplet states rapidly decay to low-lying 1s2s ^{3}S, 1s2s ^{1}S and 1s2p ^{1}P atomic excited states by droplet-induced transitions followed by ICD between pairs of these states and multi-step ionization, accordingly. In medium-sized He nanodroplets, a pronounced broadening of the electron spectra is observed due to an increase of the total number of created ICD electrons causing space charge effects. For large He nanodroplets, inelastic electron scattering plays a significant role and a cold, dense nanoplasma forms. Furthermore, when more than two electronically excited atoms are involved, the ionization dynamics develops from two-body ICD to collective autoionization (CAI) and higher-order CAI, and/or thermal electron emission dominates.

We find the best match between the simulations and the experimental data consistently in the full range of the experimental parameters when assuming a characteristic ICD time of 500 fs.

In the intensity range of the present study, where the excitation density is rather high, the ionisation dynamics is determined by the number of excited He atoms per He droplet rather than by the density of excitations.

Furthermore, our simulation indicates that the transition from two-body ICD to many-body CAI occurs at about 2.5% excitations per droplet. Thus, our results provide a detailed understanding of how autoionization of droplets evolves from a regime of low numbers of excitations in the droplets characterized

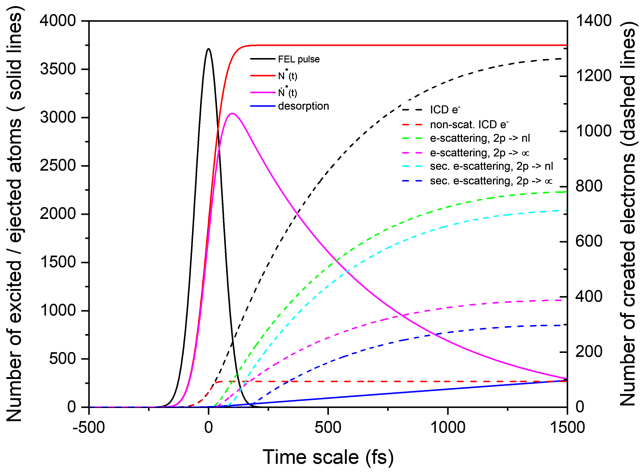

Figure A2. Simulated ionization dynamics of 1s2p $^1P_1$ excited states within $He_{50\,000}$ nanodroplets by130 fs FEL pulses (solid black line, –) at $I = 7.5 \times 10^{10}$ W cm^{-2}. The total number of excited atoms is shown by the solid red (–) line. The solid blue line (–) shows the desorption process. The evolution of excited states is given by the solid magenta (–) line, which represents the number of He^* atoms after both ICD decay and desorption of He^* atoms. Total number of created ICD electrons (ICD e^-) and discrete number of non-scattered ICD electrons (non-scat. ICD e^-) are shown by the dashed black (--) and dashed red (--) lines, respectively. Inelastic electron-impact excitations of the 2p excited state to high-lying *nl* levels (e-scattering, $2p \rightarrow nl$) is given by the dashed green (--) line. Inelastic electron-impact excitations of the 2p excited state to the continuum (e-scattering, $2p \rightarrow \infty$) is shown by the dashed magenta (--) line. Secondary scattering processes corresponding to $2p \rightarrow nl$ and $2p \rightarrow \infty$ transitions represented by the dashed cyan (--) and dashed blue (--) lines, respectively.

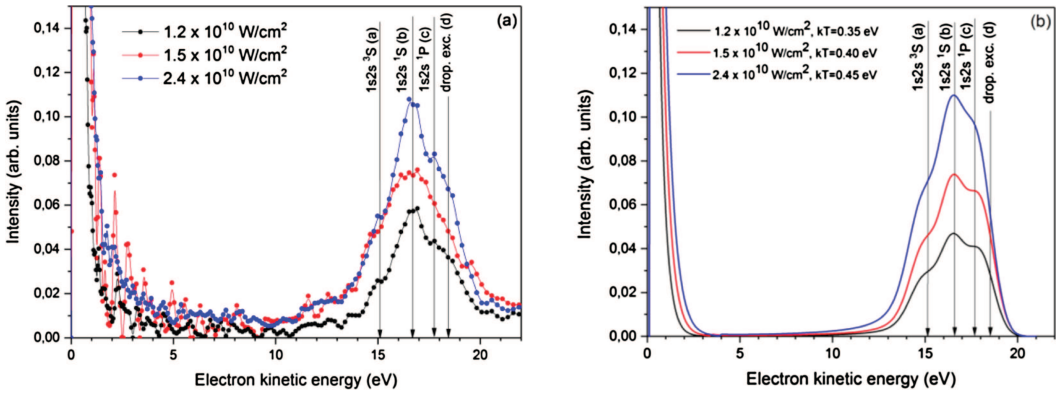

Figure A3. Electron spectra of small He droplets irradiated at $h\nu = 21.5$ eV and low power densities: (a) experimental results for He droplet size of $\langle N \rangle = 250$ atoms; (b) numerical simulations for He droplet size of $N = 250$ atoms. Maxima (a), (b) and (c) correspond to ICD of pairs of 1s2s ^{3}S, 1s2s ^{1}S and 1s2p ^{1}P atomic states [18] within a droplet, respectively. Feature (d) is caused by ICD of droplet excited states and direct photoionization of the He atomic beam.

by sharp electron emission lines, to complex autoionization involving many different processes, which eventually results in a cold dense plasma emitting electrons with a broad energy distribution. By comparing the experimental results with our simulations, we identify several interesting, fundamental questions which still remain open. Namely, what happens on ultrafast time scales, can we observe the migration or diffusion of excitations? How does a transition from delocalized to localized states take place? How does a network of excitations and subsequent plasma dynamics develop? While these topics need in the first place more detailed theoretical work, from an experimental point of view, performing time resolved measurements to directly access the complete time evolution of the system is highly desirable and will give direct insight into the motion of excitations, such as bubble formation followed by ejection of the excitation out of the droplet or even merging of bubbles.

Acknowledgments

The authors would like to thank P Demekhin, K Gokhberg, LS Cederbaum, T Fennel, U Saalmann and N Sisourat for enlightening discussions. The support of the FERMI staff and financial support by the Deutsche

Forschungsgemeinschaft within projects MO 719/14-1, and MO 719/14-2, STI 125/19-1 and MU 2347/12-1 (Priority Programme 1840 'QUTIF'), and Carlsberg Foundation are gratefully acknowledged. DI acknowledges support by IMRAM, Tohoku University, KU acknowledges support by the XFEL Priority Strategy Program MEXT and the TAGEN project while TN and KU acknowledge support by the Research Program of 'Dynamic Alliance for Open Innovation Bridging Human, Environment and Materials' in 'Network Joint Research Center for Materials and Devices'.

ORCID iDs

Y Ovcharenko https://orcid.org/0000-0001-6804-9781
B Langbehn https://orcid.org/0000-0002-3245-8169
R Cucini https://orcid.org/0000-0001-8516-1409
M Coreno https://orcid.org/0000-0003-4376-808X
C Callegari https://orcid.org/0000-0001-5491-7752
K C Prince https://orcid.org/0000-0002-5416-7354
F Stienkemeier https://orcid.org/0000-0001-6014-8013
M Mudrich https://orcid.org/0000-0003-4959-5220

References

[1] Ayvazyan V *et al* 2002 *Phys. Rev. Lett.* **88** 104802
[2] Emma P *et al* 2010 *Nat. Photon.* **4** 641–7
[3] Allaria E *et al* 2012 *Nat. Photon.* **6** 699–704
[4] Wabnitz H *et al* 2002 *Nature* **420** 482
[5] Shintake T *et al* 2008 *Nat. Photon.* **2** 555–9
[6] Hoener M *et al* 2010 *Phys. Rev. Lett.* **104** 253002
[7] Sorokin A *et al* 2007 *Phys. Rev. Lett.* **99** 213002
[8] Saalmann U and Rost J-M 2002 *Phys. Rev. Lett.* **89** 143401
[9] Schorb S *et al* 2012 *Phys. Rev. Lett.* **108** 233401
[10] Bostedt C *et al* 2010 *New J. Phys.* **12** 083004
[11] Bostedt C *et al* 2008 *Phys. Rev. Lett.* **100** 133401
[12] Gaffney K J and Chapman H N 2007 *Science* **316** 1444
[13] Santra R *et al* 2000 *Phys. Rev. Lett.* **85** 4490
[14] Kuleff A I *et al* 2010 *Phys. Rev. Lett.* **105** 043004
[15] Jahnke T 2015 *J. Phys. B: At. Mol. Opt. Phys.* **48** 082001
[16] Marburger S *et al* 2003 *Phys. Rev. Lett.* **90** 203401
[17] Hergenhahn U 2011 *J. Electron Spectrosc. Relat. Phenom.* **184** 78
[18] Buchta D *et al* 2013 *J. Chem. Phys.* **139** 084301
[19] Penning F M 1927 *Naturwissenschaften* **15** 818
[20] Katsuura K 1965 *J. Chem. Phys.* **42** 3771
[21] Djrerad M T 1992 *J. Phys. Chem.* **97** 8334
[22] Shriever K E 1987 *Phys. Rev. Lett.* **59** 1906
[23] Kuno M *et al* 2003 *Phys. Rev.* B **67** 125304
[24] Averbukh V, Müller I B and Cederbaum L S 2004 *Phys. Rev. Lett.* **93** 263002
[25] Ben Ltaief L *et al* 2019 *J. Phys. Chem. Lett.* **10** 6904
[26] Ovcharenko Y *et al* 2014 *Phys. Rev. Lett.* **112** 073401
[27] Laarmann T *et al* 2004 *Phys. Rev. Lett.* **92** 143401
[28] Nagaya K *et al* 2013 *J. Phys.* B **46** 164023
[29] Yase S *et al* 2013 *Phys. Rev.* A **88** 043203
[30] LaForge A *et al* 2014 *Sci. Rep.* **4** 3621
[31] Joppien M, Karnbach R and Möller T 1993 *Phys. Rev. Lett.* **71** 2654
[32] Nagaya K *et al* 2016 *Nat. Commun.* **7** 13477
[33] Karnbach R *et al* 1993 *Rev. Sci. Instrum.* **64** 2838
[34] Toennies J and Vilesov A 2004 *Angew. Chem., Int. Ed.* **43** 2622
[35] Harms J, Toennies J P and Dalvolvo F 1998 *Phys. Rev.* B **58** 3341
[36] Lyamayev V *et al* 2013 *J. Phys.* B **46** 164007
[37] Svetina C *et al* 2012 *Proc. SPIE* **8503** 850302
[38] Zangrando M *et al* 2009 *Rev. Sci. Instrum.* **80** 113110
[39] Gomez L *et al* 2011 *J. Chem. Phys.* **135** 154201
[40] Hagena O F 1987 *Z. Phys.* D **4** 291
[41] Buck U and Krohne R 1996 *J. Chem. Phys.* **105** 5408
[42] Garcia G A, Nahon L and Powis I 2004 *Rev. Sci. Instrum.* **75** 4989
[43] Arbeiter M and Fennel T 2010 *Phys. Rev.* A **82** 013201
[44] Arbeiter M and Fennel T 2011 *New J. Phys.* **13** 053022
[45] Saalmann U, Siedschlag C and Rost J M 2006 *J. Phys.* B **39** R39
[46] Fennel T *et al* 2010 *Rev. Mod. Phys.* **82** 1793
[47] Möller T *et al* 1999 *Eur. Phys. J.* D **9** 5–9
[48] Jacobs V L 1974 *Phys. Rev.* A **9** 1974

[49] Ziemkiewicz M P et al 2015 Int. Rev. Phys. Chem. 34 239
[50] Mudrich M et al 2020 Nat. Commun. 11 112
[51] Iablonskyi D et al 2016 Phys. Rev. Lett. 117 276806
[52] Serdobintsev P Y et al 2018 J. Chem. Phys. 148 194301
[53] Ralchenko Y et al 2008 At. Data Nucl. Data Tables 94 603
[54] Ziemkiewicz M P et al 2015 Int. Rev. Phys. Chem. 34 239–67
[55] Keller W E 1969 Helium-3 and Helium-4 (New York: Plenum Press) https://doi.org/10.1007/978-1-4899-6485-4
[56] von Haeften K et al 1997 Phys. Rev. Lett. 78 4371
[57] von Haeften K et al 2002 Phys. Rev. Lett. 88 233401
[58] Stauffer D and Aharony A 1994 Introduction to Percolation Theory (Boca Raton, FL: CRC Press)